Nonequilibrium $c(2\times2)$ island formation during chemisorption: Scaling of spatial correlations and diffracted intensity

J. W. Evans, R. S. Nord,* and J. A. Rabaey
Ames Laboratory, Iowa State University, Ames, Iowa 50011
(Received 4 November 1987)

During chemisorption, islands often form in which adspecies have superlattice spacing. Upon meeting, these coalesce if in phase, and form a domain boundary otherwise. Manifestly nonequilibrium island distributions can develop as a result of kinetic limitations, and a metastable saturation state of domain boundaries may, in turn, result. We analyze irreversible cooperative filling models for the formation of $c(2\times2)$ islands, where island structure is kinetically determined, and extensive coalescence near saturation produces a "percolative" domain structure. We show that the associated dramatic increase in domain size, and fractal domain structure, are *not* reflected in the spatial pair-correlation or diffracted-intensity behavior. Consequently, we identify quasi-one-dimensional measures of domain size which better reflect correlation-length behavior. These are then used to develop scaling relations for pair correlations and diffracted intensities. A special case of our model describes metastable $c(2\times2)$O/Fe(001) formed after exposure of Fe(001) to H_2O.

I. INTRODUCTION

Many chemisorption systems exhibit a propensity for island formation.[1] Often adspecies constituting these islands have superlattice spacing, in which case they reside on one of several adsorption-site sublattices, and are assigned a "phase" accordingly. Figure 1 depicts $\sqrt{2}\times\sqrt{2}R45°$ or $c(2\times2)$ islands on a square lattice, which have one of two phases. Here we consider the evolution of such order during chemisorption, i.e., with increasing coverage, Θ. Such processes involve competition between nucleation and growth of islands, as well as coalescence of in-phase islands, and the formation of domain boundaries between out-of-phase islands (see Fig. 1). Such adlayer states may be far from equilibrium due to kinetic limitations of low surface mobility.[2] This implies that the structure of the growing islands is at least, in part, kinetically determined, and that the process may well generate a "metastable saturation state," with no long-range order, in which only domain boundaries separate islands of different phase.

There are available many sophisticated analyses of adlayer statistics for the equilibrium state.[3] Several nonequilibrium studies have characterized the dynamics of equilibration at constant coverage, Θ, following a rapid quench. Various evolution mechanisms associated with first-order transitions, as well as order-disorder transitions, have been studied, focusing on the time dependence of late-stage growth.[4] However there are very few treatments of nonequilibrium island formation or ordering during chemisorption,[5–8] the topic of this investigation.

The statistics or structure of island formation during chemisorption is naturally characterized in terms of three (possibly) distinct length scales:

(i) On the scale of a few lattice vectors, probabilities of various local configurations determine such quantities as the sticking probability, island edge densities, etc., as functions of the time (t) or coverage (Θ).

(ii) The characteristic or correlation length measures the rate of decay of the spatial pair correlations. It also gives a measure of the average island size, provided coalescence does not have a significant effect. Island structure on this length scale, including shape, boundary structure, and growing or active zone width, is strongly dependent on the details of the growth process. The island growth rate could be mediated either by the rate of chemisorption from the precursor, or by diffusion. If growth is *not* diffusion mediated, then local growth rules produce regular structures. For diffusion-mediated growth, intraisland rearrangement will probably quench any Mullins-Sekerka–type shape instabilities,[9] thus also resulting in regular structures.

(iii) The connectivity length measures the domain ra-

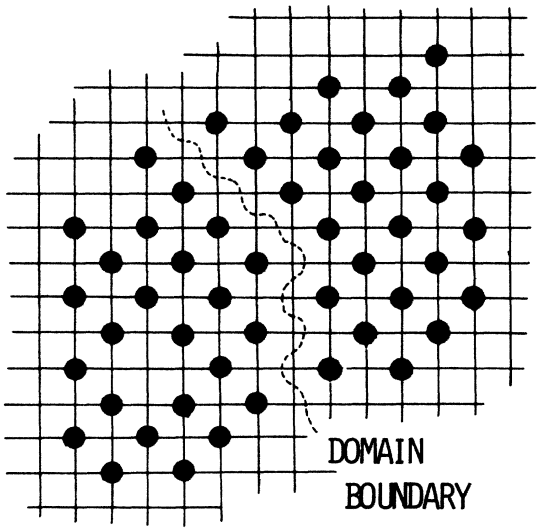

FIG. 1. Two $c(2\times2)$ islands of different phase separated by a domain boundary. One atom is missing from the interior of the island on the right, creating a "$p(2\times2)$ defect."

dius of gyration, and can be much larger than the correlation length if many islands have coalesced. This is typically the case for $c(2\times2)$ islands near saturation, where domains exhibit an interpenetrating and nested percolation-cluster-like structure.[7,8] The fractal-like structure of domains, and probably their boundaries, on this large length scale is less model dependent, being dictated by the random percolation universality class for the nonequilibrium models considered here. See Ref. 8 for more detail.

Low-energy electron diffraction (LEED) is commonly used to analyze adlayer and, specifically, island structure.[10] The simplest island-size-broadening model (ISBM) for kinematic scattering only from the adlayer assumes no interference between the scattered intensity from different islands in the vicinity of the superlattice beam.[2] The ISBM superlattice beam peak intensity measures a certain average of the island size, and the full width at half maximum (FWHM) reflects the linear dimension. The ISBM should apply for separated, regular islands. However, near saturation, interference is undoubtedly significant.[11,12] More fundamentally, since the diffracted intensity is determined by the pair correlations, it reflects structure on the correlation, *not* connectivity, length scale. Correspondingly, we shall see that the superlattice beam behavior does *not* reflect the dramatic increase in domain size associated with significant coalescence near saturation, or the associated fractal domain structure on the connectivity length scale. This fractal structure, which results from the essentially random coalescence of like-phase islands, is not visible in the pair correlations. (Similarly, the fractal structure of random percolation is obviously *not* visible in the identically zero pair correlations.) One objective of this work will be to identify measures of island size whose behavior better parallels that of the correlation length, and thus of the diffracted intensity.

Here we consider models for irreversible, immobile chemisorption from a mobile physisorbed precursor "source" of density, ρ. The chemisorption rates are assumed to include ρ as a factor. Island formation is associated with enhanced rates for chemisorption at island edges (these rates determine the structure of growing islands) relative to the rate for chemisorption in empty regions (homogeneous island nucleation). This enhancement in the rates could reflect enhancement of the precursor source density, ρ, near island edges. This, in turn, is associated with an increase in the precursor binding energy $J(\mathbf{r})$ at such sites $\mathbf{r}$ due to attractive interactions with chemisorbed species.[6] Note that for a low-density equilibrated precursor, one has $\rho \sim e^{\beta J(\mathbf{r})}$. Such attractive interactions could also reduce any activation energy barrier to chemisorption, further enhancing island formation. Note that any time dependence in the spatial average of ρ would modulate all chemisorption rates, but not affect adlayer statistics, and is thus not discussed further here.

More specifically, we analyze irreversible cooperative chemisorption models, wherein chemisorption occurs filling single sites which have *no* occupied nearest neighbors (NN's), with rates k_i depending on the number i of already occupied next-nearest-neighbor (NNN) sites. Chemisorbed species are assumed immobile. These models generate $c(2\times2)$ ordering on a square lattice (where NNN sites are the diagonal NN sites) or double-spaced islands on a linear lattice, with no long-range order. They produce a metastable saturation state with $\Theta=\Theta^*<\frac{1}{2}$, where no empty sites remain with all NN's empty, and islands are separated only by domain boundaries. It will be instructive here to consider *classes* of models parametrized by the growth to nucleation rate ratio $\alpha=k_1/k_0$. Clearly, as α increases (for fixed Θ or at saturation), the correlation length and any measure of island size also increase. The $\alpha\rightarrow\infty$ limit corresponds to continuum models of island growth.

As indicated above, in this contribution we identify quasi-one-dimensional measures of island size which behave similarly to the correlation length (even for these models with percolative ordering). These are then used as characteristic or scaling lengths in our development of scaling relations for the spatial pair correlations and diffracted intensity. We are interested in the scaling behavior associated with self-similarity in a class of models with various α (at fixed Θ or at saturation), as well as more conventional but imprecise scaling with varying Θ or time (for a specific α). Because of the complexity of these physical two-dimensional chemisorption models, we begin in Sec. II with an analysis of their one-dimensional analogues for the evolution of double-spaced islands on a linear lattice. Here exact solutions are available,[12–14] and many of the basic questions concerning scaling and the effect of coalescence can be explored. In Sec. III, we return to analysis of the two-dimensional models for evolution of $c(2\times2)$ islands on a square lattice. Computer simulation is now used to determine all quantities of interest. Different rate choices generate islands with either narrow or broad growing (or active) zones, which affects our specification of the scaling length. The dramatic effects of percolative island coalescence are described. We also discuss the case of random filling with NN blocking ($\alpha=1$) modeling metastable $c(2\times2)$O/Fe(001) formed after exposure of Fe(001) to H_2O.[15] Finally, in Sec. IV we review our findings, and emphasize their applicability to various other models of $c(2\times2)$ ordering. We also note the reduced propensity for coalescence if islands have several phases, and the increased propensity in three dimensions.

II. EVOLUTION OF DOUBLE-SPACED ISLANDS ON A LINEAR LATTICE

Here irreversible chemisorption o$\rightarrow$x occurs at single sites with both NN's empty with rates k_i depending on the number i of occupied NNN's. Thus k_0 corresponds to island nucleation, k_1 to growth, and k_2 to coalescence. Double-spaced islands can meet either in phase [$\cdots$ oxoxoooxoxo $\cdots$, where the center o site fills if $k_2\neq0$], or out of phase [$\cdots$ oxoxooxoxo $\cdots$], creating a permanent domain boundary. The saturation state contains no empty triples, and its statistics are independent of $k_2\neq0$. Let n_s denote the probability of an island [ooxoxo $\cdots$ oxoxoo] with exactly s filled sites, so

$\sum_s sn_s = \Theta$, and $\sum_s n_s = P[\text{xoo}] = P[\text{oox}] = P[\text{oo}] - P[\text{ooo}] = 1 - 2\Theta - P[\text{ooo}] \equiv D$, the island density. Here P's denote subconfiguration probabilities. Average island size can be defined as $s'_{\text{av}} = \sum_s sn_s / \sum_s n_s$ or $s_{\text{av}} = \sum_s s^2 n_s / \sum_s sn_s$ ($\geq s'_{\text{av}}$). Note that $s'_{\text{av}} = \Theta/D \to \Theta^*(1-2\Theta^*)^{-1}$ at saturation. Results below are obtained from exact truncation of the hierarchial form of the master equations.[12-14]

We shall focus on the behavior of this model in the strongly clustering regime where the ratio of growth to nucleation rates, $\alpha = k_1/k_0$, is large. Here fluctuations in island growth become less significant, justifying a picture in which islands have edges expanding at constant rate $2\alpha k_0$ lattice vectors per unit time (after nucleation at rate k_0). Using this picture,[7] one can show that characteristic or scaling length, ξ, and characteristic time, τ, satisfy $\xi \sim c(\Theta)\alpha^{1/2}$, where $c \sim \Theta^{1/2}$, as $\Theta \to 0$, and $\tau \sim k_0^{-1}\alpha^{-1/2}$. The corresponding $\alpha^{1/2}$ scaling of s'_{av}, both at fixed Θ and saturation, and the relation $\frac{1}{2} - \Theta^* \sim \frac{1}{8}(2\alpha/\pi)^{-1/2}$, have been confirmed previously.[7]

More complete information on the large-α self-similar structure follows from various scaling functions, e.g., $n_s \sim \xi^{-1} F(y = s/\xi, \Theta/\Theta^*)$, which establishes the proportionality of $s'_{\text{av}} \sim \xi \int dy\, yF / \int dy\, F$ and $s_{\text{av}} \sim \xi \int dy\, y^2 F / \int dy\, y\, F$. These functions are determined by a continuum two-state Johnson-Mehl model:[7,16] grains nucleate at a constant rate randomly at empty points on the line and expand at constant rate; they are randomly assigned one of two phases, and when grains meet they merge if of like phase and form a domain boundary otherwise.

We focus on the structure of the spatial pair correlation $C(l) \equiv P(l) - \Theta^2$, where $P(l)$ is the probability that a pair of sites separated by l lattice vectors are filled. These alternate in sign, and have a large-α scaling form

$$C(l) \sim \begin{cases} C^+(l/\xi, \Theta/\Theta^*) \geq 0 & \text{for } l \text{ even}, \quad (2.1a) \\ C^-(l/\xi, \Theta/\Theta^*) \leq 0 & \text{for } l \text{ odd}, \quad (2.1b) \end{cases}$$

associated with self-similarity of distributions for various α, at fixed $x = \Theta/\Theta^*$. Since $C(0) = \Theta - \Theta^2$ and $C(1) = -\Theta^2$, one finds that $C^+(0,x) = x/2 - x^2/4$ and $C^-(0,x) = -x^2/4$. As $x \to 0$, one finds $C^-/C^+ \to 0$, and the C^+ correspond to intraisland correlations.[12] At saturation ($x = 1$) consecutive correlations tend to cancel for large α,[7,12] so $C^+(y,1) + C^-(y,1) = 0$. Clearly we could choose ξ as s_{av} or s'_{av} in this discussion. To determine how quickly low-α correlations approach the high-α scaling form, in Fig. 2 we have shown $C(l)$ versus l/s_{av} for $\alpha = 1,2,5,10,40$ at both half-saturation and saturation. The high-α form is achieved for $\alpha \gtrsim 15$, and low-α $C(l)$ scale best at saturation. Similar behavior results using s'_{av} rather than s_{av}.

Next we consider scaling of the angular distribution of the diffracted intensity, $I(q)$, in these models for kinematic scattering from the adlayer only. Here, $q = \Delta\mathbf{k} \cdot \mathbf{a}$, where $\Delta\mathbf{k}$ is the momentum transfer, and $\mathbf{a}$ is the lattice vector. With $C(-l) \equiv C(l)$, for $q \neq 0 \pmod{2\pi}$ one has that

$$\Theta I(q) = \sum_l e^{iql} C(l) , \quad (2.2)$$

normalizing I to unity as $\Theta \to 0$. We must separately scale the integral-order (I_0) and superlattice or half-order ($I_{1/2}$) beam intensities, centered on $q = 0 \pmod{2\pi}$ and $q = \pi \pmod{2\pi}$, respectively. Set $q' = q - \pi$. Then, for small q and q', Eqs. (2.1) and (2.2) imply that

$$\begin{aligned} I_0(q) &\sim \xi G^+(\xi q, \Theta/\Theta^*) , \\ I_{1/2}(q') &\sim \xi G^-(\xi q', \Theta/\Theta^*) , \end{aligned} \quad (2.3)$$

where $G^{\pm}(p,x) = \int_0^\infty dy \cos(py) F^{\pm}(y,x)$ and $F^{\pm} = 2x^{-1}[C^+(y,x) \pm C^-(y,x)]$. Note that $F^-(0,x) = 1$ for all x, $F^+(0,x) = 1 - x$, and $F^+(y,1) \equiv 0$, so that $I_0 = 0$ and $I = I_{1/2}$ at saturation ($x = 1$).

Behavior of $I_{1/2}/s_{\text{av}}$ versus $s_{\text{av}} q'$ at saturation for $\alpha = 1,2,5,40$ is shown in Fig. 3. There is little deviation from the high-α form. For $\alpha < \infty$, determination of $I_{1/2}$ below saturation requires first deconvoluting $I = I_0 + I_{1/2}$ into components. Here we take $I_0(q)$ of the form

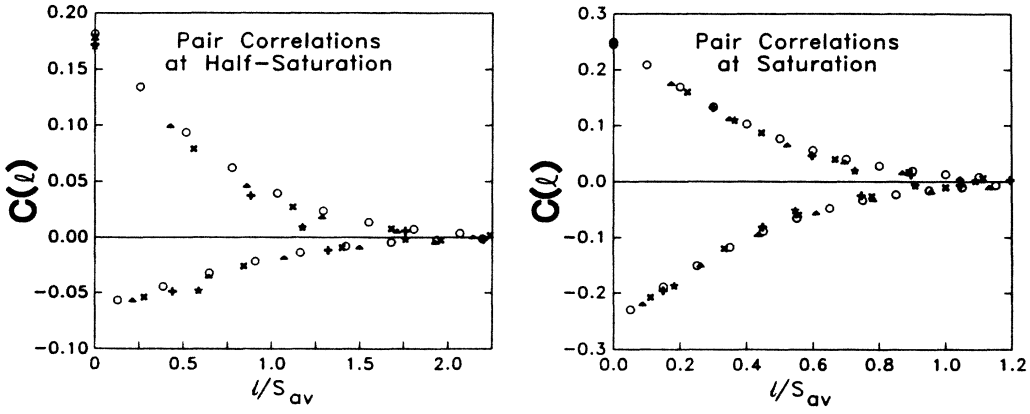

FIG. 2. $C(l)$ vs l/s_{av} for double-spaced islands on a linear lattice at half-saturation and saturation. Results are shown for $k_i \propto \alpha^i$ with $\alpha = 1$ (★), 2 (+), 5 (×), 10 (▲), and 40 (○).

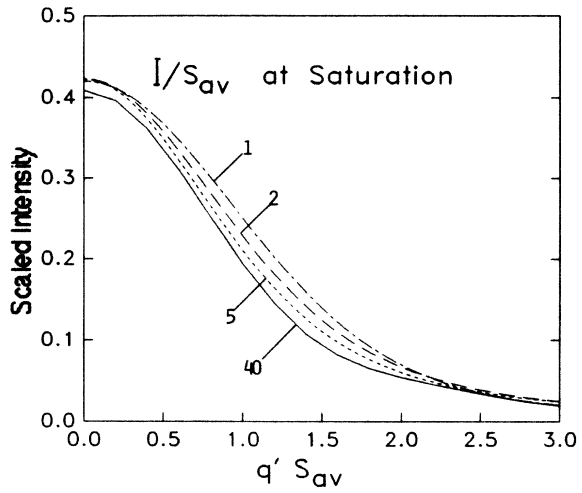

FIG. 3. $I_{1/2}/s_{av}$ $(=I/s_{av})$ vs $s_{av}q'$ for double-spaced islands at saturation and various α (shown).

$A\sum_m G^+(\lambda(q-2m\pi))$ determining $A(\lambda)$ by matching the peak intensity (curvature) of I at $q=0$;[17] this automatically determines $I_{1/2}$. Applying this procedure for $\alpha=2$ at half-saturation (Fig. 4) reveals $I_{1/2}$ scaling comparable to that at saturation. Note that even if the correlations were to scale perfectly, the occurrence of a discrete sum (rather than an integral) in (2.2) would produce deviations in intensity scaling.

From such analyses we can extract the coverage dependence of the q-space FWHM of $I_{1/2}$, denoted $W_{\rm FWHM}$. In Fig. 5 we have shown $W_{\rm FWHM}s_{av}$ and $W_{\rm FWHM}2s'_{av}$ versus $x=\Theta/\Theta^*$. In the large-α, large-island-size regime, these quantities increase smoothly from low-Θ values of $\sim\pi$ to saturation values of $\sim2\pi$. One should contrast this with the behavior for corresponding second-order, spatially Markovian distributions (i.e., equilibrium distributions for range-2 interactions incorporating infinite NN repulsions) where $s_{av}=s'_{av}(2$

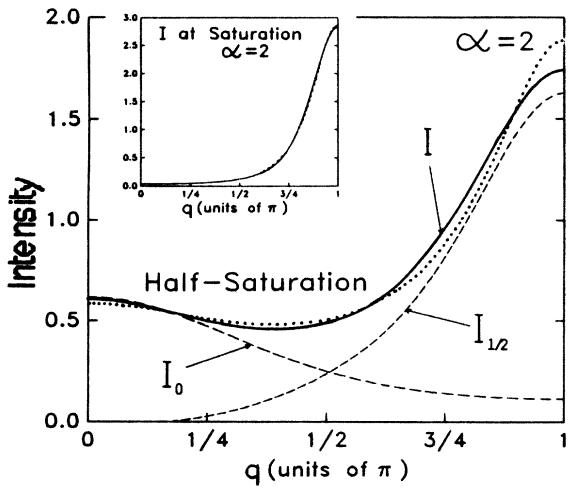

FIG. 4. Deconvolution of $I(q)$ into integral-order (I_0) and superlattice $(I_{1/2})$ components at half-saturation for $\alpha=2$. We have also shown $I(q)$ for double-spaced island distributions with second-order Markovian statistics, having the same Θ and s'_{av} as the chemisorption process (dotted lines).

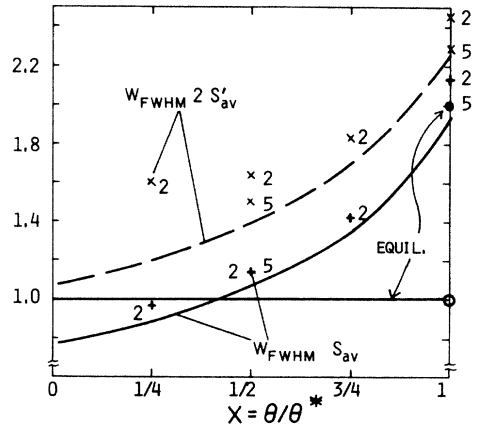

FIG. 5. $W_{\rm FWHM}s_{av}$ and $W_{\rm FWHM}2s'_{av}$ vs $x=\Theta/\Theta^*$ for double-spaced islands. The q-space FWHM of $I_{1/2}$ is measured in units of π. Curves correspond to large-α $(=40)$ behavior, and some $\alpha=2$ and 5 values are shown. Corresponding large s'_{av} equilibrium (second-order Markov) results are also shown.

$-(s'_{av})^{-1})\sim2s'_{av}$, as $s_{av}\to\infty$. Here these products are constant at unity for fixed Θ (below saturation), but jump to 2 at saturation (see Appendix A). Thus the nonequilibrium behavior seems to bridge the $\Theta=0$ and $\Theta=1$ equilibrium limits. One can also consider the coverage dependence of the superlattice beam peak intensity for large island sizes. For large α, $I(\pi)/s_{av}[I(\pi)/(2s'_{av})]$ increases roughly linearly from 0.4 (0.35) at saturation to 1.0 (0.7) for low Θ. Compare this with equilibrium values of $\frac{1}{2}$ (1) at (below) saturation. Note that, in the *low-Θ regime* there is no significant interference between scattering from different islands, even for large s_{av}. Consequently, the island-size-broadening model[2,12] applies here to yield

$$I(q)\sim\Theta^{-1}\sum_s n_s\sin^2(sq)/\sin^2q\to s_{av}\ ,$$

as $q\to0$ or π, compatible with our results. At this point we also note that an exact Taylor-series expansion in Θ can be obtained for $I(q)$, for any fixed α (see Appendix B).

The *effect of island coalescence* on average island size and diffracted intensity behavior is finally considered here. Clearly, at low Θ the increase in average size is predominantly due to the growth of separated islands, whereas at higher Θ coalescence of in-phase islands contributes significantly. To quantify the latter, it is convenient to compare island sizes for the above process with coalescence to those for a *modified* filling process where no island coalescence occurs (i.e., set $k_2=0$). Below, (C) and (NC) indicate values for processes with and without coalescence, respectively. In the $\alpha\to\infty$ *large-island-size regime,* the diffracted intensity is not sensitive to coalescence, i.e., $I(\mathrm{C})\sim I(\mathrm{NC})$. However, although $s_{av}(\mathrm{C})/s_{av}(\mathrm{NC})\sim s'_{av}(\mathrm{C})/s'_{av}(\mathrm{NC})\sim1$ for low Θ, one finds that at saturation $s'_{av}(\mathrm{C})/s'_{av}(\mathrm{NC})=2$ exactly, and we estimate that $s_{av}(\mathrm{C})/s_{av}(\mathrm{NC})\approx2.6$ (see Fig. 6). Comparing Figs. 5 and 6, we see that $W_{\rm FWHM}s_{av}(\mathrm{NC})$ or $W_{\rm FWHM}s'_{av}(\mathrm{NC})$ have much weaker Θ dependence than

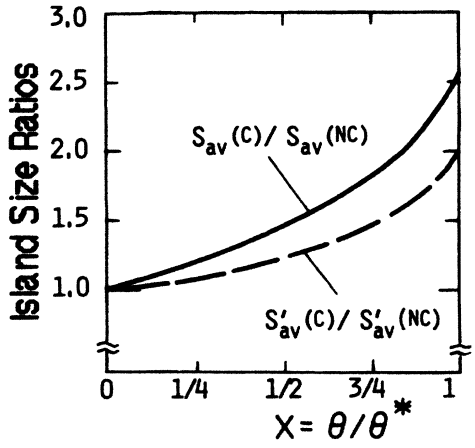

FIG. 6. Comparison of double-spaced island-size variation with $x=\Theta/\Theta^*$, for filling processes with (C) and without (NC) coalescence, in the large-island-size regime.

$W_{FWHM}s_{av}(C)$ or $W_{FWHM}s'_{av}(C)$. Furthermore, in Fig. 7 we have shown that the form of $I_{1/2}(NC)/s_{av}(NC)$ versus $s_{av}(NC)q'$ is roughly coverage independent for $\alpha=k_1/k_0=80$, i.e., $s_{av}(NC)$ [or $s'_{av}(NC)$] is the optimum choice for scaling length.

In summary, the decrease in the FWHM (or increase in peak intensity) of the superlattice beam with Θ reflects most accurately the component of the increase in island size due to growth rather than coalescence.

III. EVOLUTION OF $c(2\times2)$ ISLANDS ON A SQUARE LATTICE

Here irreversible chemisorption $o\rightarrow x$ occurs at single sites with all four NN's empty with rates k_i depending on the number i of occupied NNN's. Thus, k_0 corresponds to island nucleation, k_1 to growth, and k_2,k_3,k_4 to growth or coalescence. The saturation state contains no

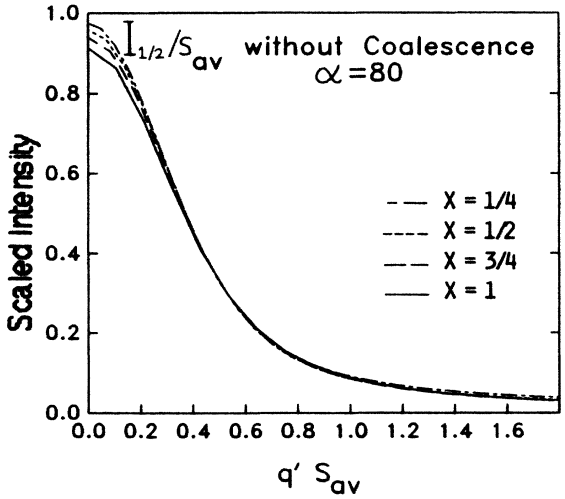

FIG. 7. Scaling of $I_{1/2}$ with $x=\Theta/\Theta^*$ for a process with no coalescence of double-spaced islands ($k_1/k_0=80$, $k_2=0$).

empty sites with all NN's empty, and its statistics are independent of $k_4\neq0$.

There are many ways to characterize $c(2\times2)$ island or domain statistics here. First, we indicate two choices of connectivity rules defining individual domains:[18] Filled sites in the same domain must be connected either directly or indirectly by (i) NNN bonds, or (ii) either NNN or third-NN bonds. Type-(ii) islands may be larger, but these definitions become equivalent in the strongly clustering regime. Numerical results following are for rule (i). Given a choice of connectivity rule, let $n_{\{s\}}$ denote the probability of a $c(2\times2)$ domain $\{s\}$ of s filled sites. Average domain size (number of filled sites) is defined as $s_{av}=\sum s^2 n_{\{s\}}/\sum s n_{\{s\}}$. Average radii of gyration can also be determined from the $n_{\{s\}}$. All these quantities are very sensitive to island coalescence. Alternatively, one can take one-dimensional cuts through the adlayer. Let m_s denote the probability of finding a horizontal (or vertical) string ooxoxo $\cdots$ oxoxoo of s adatoms, and set

$$m'_{av}=\sum s m_s\Big/\sum m_s$$
$$=\Theta/P[\text{oox}]=\Theta(1-2\Theta-P[\text{ooo}])^{-1}$$

and

$$m_{av}=\sum s^2 m_s\Big/\sum s m_s\ .$$

One can also consider the distribution of adatoms in diagonal strings consecutive filled sites, and define $m'_{avd}=\Theta/P[_o{}^x]=\Theta(\Theta-P[_o{}^o])^{-1}$ and m_{avd} analogously. We shall make use of these and other measures of domain size.

Again we mostly focus on behavior in the strongly clustering regime where the ratio of growth to nucleation rates, $\alpha=k_1/k_0$, is large. Here the scaling of the characteristic length, ξ, with α, and its relationship to the above-mentioned island-size measures, depends on the choice of k_2, k_3, and k_4. Two special cases are discussed below, but first we provide a general description of the associated pair correlation and diffracted intensity scaling.

The spatial pair correlations are defined as $C(l)\equiv P(l)-\Theta^2$, where $P(l)$ is the probability of finding a pair of filled sites separated by $l=(l_x,l_y)$ lattice vectors. These are positive (negative) when l connects sites on the same (different) $c(2\times2)$ sublattices. In the strongly clustering regime, they should exhibit the scaling form

$$C(l)\sim\begin{cases}C^+(l/\xi,\Theta/\Theta^*)\geq0 & \text{for } l_x+l_y \text{ even}\ , \quad (3.1a)\\ C^-(l/\xi,\Theta/\Theta^*)\leq0 & \text{for } l_x+l_y \text{ odd}\ , \quad (3.1b)\end{cases}$$

associated with self-similarity for various α, at fixed $x=\Theta/\Theta^*$. This scaling assumes regular rather than fractal islands before coalescence, since, in the latter case, intraisland correlations do not satisfy (3.1).[19] Since $C(0,0)=\Theta-\Theta^2$ and $C(0,1)=-\Theta^2$, one has $C^+(0,x)=x/2-x^2/4$ and $C^-(0,x)=-x^2/4$. As $x\rightarrow0$, one finds that $C^-/C^+\rightarrow0$, and the C^+ correspond to intraisland correlations.[12] At saturation, where $C(l)$ for adjacent l tend to cancel for large α,[7,12] one finds that $C^+(\mathbf{y},1)+C^-(\mathbf{y},1)=0$ (cf. Sec. II).

Next consider the diffracted intensity, $I(\mathbf{q})$, for kinematic scattering from the adlayer only. Here $\mathbf{q}=a\,\Delta\mathbf{k}$, where $\Delta\mathbf{k}$ is the lateral momentum transfer and a is the lattice constant. With $C(-l)\equiv C(l)$ and $\mathbf{q}\neq(2m\pi, 2n\pi)$, then one has that

$$\Theta I(\mathbf{q})=\sum_l e^{i\mathbf{q}\cdot l}C(l)\ , \tag{3.2}$$

normalizing I to unity as $\Theta\to0$. We must separately scale the integral-order ($I_{0,0}$) and superlattice or half-order ($I_{1/2,1/2}$) beam intensities centered at $\mathbf{q}=0$ and $\mathbf{q}'\equiv\mathbf{q}-(\pi,\pi)=0$, respectively. Equations (3.1) and (3.2) imply that

$$\begin{aligned} I_{0,0}(\mathbf{q})&\sim\xi^2G^+(\xi\mathbf{q},\,\Theta/\Theta^*)\ ,\\ I_{1/2,1/2}(\mathbf{q}')&\sim\xi^2G^-(\xi\mathbf{q}',\,\Theta/\Theta^*)\ , \end{aligned} \tag{3.3}$$

where

$$G^{\pm}(\mathbf{p},x)=\int\int d\mathbf{y}\,x^{-1}[C^+(\mathbf{y},x)\pm C^-(\mathbf{y},x)]e^{i\mathbf{p}\cdot\mathbf{y}}\ .$$

Clearly, one has $I_{0,0}=0$, so $I=I_{1/2,1/2}$, at saturation. Below saturation, we deconvolute I into 0,0 and $\frac{1}{2},\frac{1}{2}$ components mimicking the one-dimensional procedure. Where practical, $I_{0,0}$ is taken as a periodic form of G^+ scaled in amplitude and width to fit the full I around $\mathbf{q}=0$. The residual part of I is taken as $I_{1/2,1/2}$.

Finally, we note that in the low-Θ regime the ISBM applies even for strongly clustering systems, and $C\sim C^+$ correspond to intraisland correlations.[12] Let

$$I_{\{s\}}(\mathbf{q})=\left|\sum_{\mathbf{r}\in\{s\}}e^{i\mathbf{q}\cdot\mathbf{r}}\right|^2$$

denote the diffracted intensity for a single island $\{s\}$, so $I_{\{s\}}\to s^2$ as $\mathbf{q}\to(0,0)$ or (π,π). In the ISBM one has

$$I(\mathbf{q})=\Theta^{-1}\sum I_{\{s\}}(\mathbf{q})n_{\{s\}}\to s_{\rm av} \quad \text{as } \mathbf{q}\to(0,0) \text{ or } (\pi,\pi)\ . \tag{3.4}$$

Remember that $s_{\rm av}$ becomes independent of the choice of island-connectivity rule in the strongly clustering regime where (3.4) holds. We also note here that exact Taylor-series expansions in Θ can be obtained for $I(\mathbf{q})$, for any choice of k_i (see Appendix B).

All numerical results presented below are obtained from computer simulation, specifically by averaging over 20 chemisorption trials on a 400×400 lattice with periodic boundary conditions. We thus obtain very-high-quality statistics for the $C(l)$, which allow accurate calculation of $I(\mathbf{q})$, even for strongly clustering systems where statistical fluctuations are larger.

A. Islands with narrow growing zones: Multiplicative rates $k_i\propto\alpha^i$

First, we indicate why, for large α, $c(2\times2)$ islands before coalescent tend to be diamond-shaped here. Consider the island in Fig. 8. Chemisorption along the kinked edge of $O(m)$ occupied sites occurs quickly via $O(m)$ filling events at rate $k_2=\alpha k_1$. Initiation of chemisorption on a smooth side occurs with rate k_1 at any of $O(m)$ sites. Thus sides tend to remain smooth if $O(k_2/m)\gg O(mk_1)$, or $m\ll O(1)\alpha^{1/2}$.

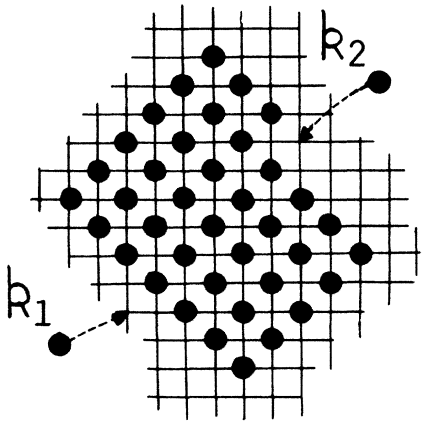

FIG. 8. Development of diamond-shaped $c(2\times2)$ islands for chemisorption with multiplicative rates, and large α.

Large-α scaling behavior is elucidated by the following picture neglecting fluctuations in island growth: islands nucleate continuously in empty regions at rate k_0; they grow with a diamond shape having edges accelerating outwards at rate $\sqrt{2}k_1m$ (where m is the number of atoms on an edge); impinging in-phase islands rapidly form a larger diamond-shaped island encompassing both via filling at rate k_2;[20] when out-of-phase islands meet, a domain boundary forms, and accelerating growth continues with the larger island tending to engulf the smaller. Some island-edge roughening is expected for higher Θ, but simulations still show a propensity for diagonal domain boundaries in the saturation state (Fig. 9).

Here the characteristic or scaling length, ξ, satisfies $\xi\sim c(\Theta)\alpha^{1/2}$ for large α, where $c\sim\Theta^{1/2}$, as $\Theta\to0$.[7] Corresponding $\alpha^{1/2}$ scaling of $m'_{\rm av}$ *both* at fixed Θ and at saturation, as well as $\alpha^{-1/2}$ scaling of $\frac{1}{2}-\Theta^*$, have also been confirmed.[7] In fact, $m_{\rm av}$, $m'_{\rm av}$, $m_{{\rm av}\,d}$, and $m'_{{\rm av}\,d}$ all scale like $\alpha^{1/2}$, and any is a reasonable candidate for the scaling length. We shall see later that this is only true below saturation because here islands have a "narrow" growing (or active) zone.

We now analyze spatial-correlation and diffracted intensity behavior for $\alpha=1,2,5,40$ to assess how quickly the high-α scaling form is achieved. Figure 10 shows $C(l,0)$ versus $l/m_{{\rm av}\,d}$ both at half-saturation and at saturation. The high-α form is achieved for $\alpha\gtrsim15$ at saturation, and scaling is generally poorer below saturation. $C(l,l)\geq0$ versus $l/m_{{\rm av}\,d}$ behaves similarly. Replacing $m_{{\rm av}\,d}$ by $m_{\rm av}$ produces poorer scaling below saturation. Figure 11 shows $I_{1/2,1/2}/m^2_{{\rm av}\,d}$ versus $m_{{\rm av}\,d}\,|\mathbf{q}'|$, for $\mathbf{q}'=(q',q')$, both at half-saturation [using the above-mentioned deconvolution procedure, except for $\alpha=1$ (Ref. 21)] and at saturation. Except for larger undulations when $\alpha=1$, corresponding $\mathbf{q}'=(q',0)$ behavior is very similar. Replacing $m_{{\rm av}\,d}$ by $m_{\rm av}$, $m'_{{\rm av}\,d}$, or $m'_{\rm av}$ has little effect on the quality of low-α intensity scaling at saturation ($m_{\rm av}$ gives the poorest results), but these replacements greatly reduce the quality below saturation.

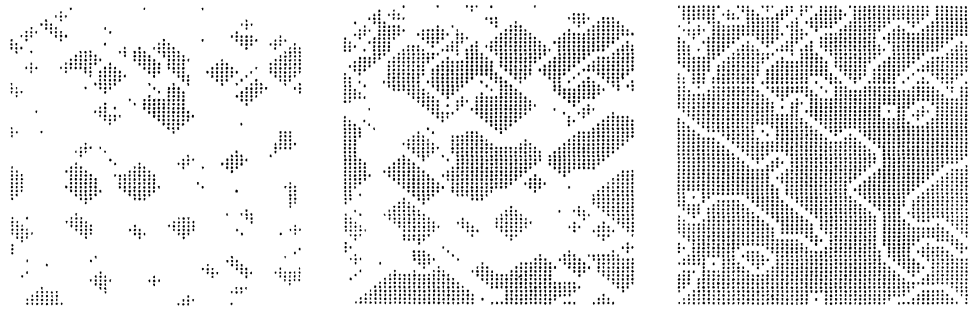

FIG. 9. Computer simulation of $c(2\times2)$ island formation for chemisorption with multiplicative rates, $k_i \propto 40^i$, for $x=\Theta/\Theta^*=\frac{1}{3},\frac{2}{3},1$. X and Y denote filled sites in domains of different phase; ○ denoting empty sites are only shown within $c(2\times2)$ domains for contrast.

Next, we analyze the coverage dependence of the FWHM for diagonal cross sections [i.e., along $\mathbf{q}'=(q',q')$] of $I_{1/2,1/2}$. $W_{\mathrm{FWHM}} m_{\mathrm{av}\,d}$ and $W_{\mathrm{FWHM}} 2m'_{\mathrm{av}\,d}$ versus $x=\Theta/\Theta^*$, shown in Fig. 12, increase smoothly from $\sim\pi$, when $x=0$, to $\sim2\pi$, when $x=1$, for large α. The FWHM for horizontal (or vertical) cross sections are very similar. We find $m_{\mathrm{av}\,d}/m_{\mathrm{av}} \approx m'_{\mathrm{av}\,d}/m'_{\mathrm{av}}$ has only weak coverage dependence, so interchange of diagonal for horizontal domain-size measures makes little difference. Finally, we analyze the coverage dependence of the superlattice beam peak intensity (Table I). For large α, $I(\pi,\pi)/m^2_{\mathrm{av}\,d}$ $[I(\pi,\pi)/(2m'_{\mathrm{av}\,d})^2]$ decreases more than fourfold with Θ to its saturation value of 0.29 (0.24). The ISBM result $I(\pi,\pi)/s_{\mathrm{av}} \to 1$, as $\Theta \to 0$, is compatible with the former since $s_{\mathrm{av}} > m^2_{\mathrm{av}\,d}$ for *distributions* of diamond-shaped islands.[22] A discussion of the effects of coalescence is left to subsection C. However, we note here that $I_{1/2,1/2}/I(\pi,\pi)$ as a function of $I(\pi,\pi)^{1/2}\mathbf{q}'$ is almost coverage independent for $\alpha=40$.

B. Islands with broad growing zones: Eden rates $k_i=\alpha k_0$ for $i \geq 1$

Here, $c(2\times2)$ islands before coalescence are Eden clusters[23] on one of the $\sqrt{2}\times\sqrt{2}R45°$ square sublattices. Consequently, these have a roughly circular, large-size shape. (This is only apparent for *very* large α.) Also their growing (or active) zone width, w, scales like their radius, R, to a power p between ~0.32 and $\frac{1}{2}$ depending on R.[23] For very large α, where fluctuations in island growth are less significant, one obtains the following picture: islands nucleate continuously in empty regions at rate k_0; roughly circular islands have radii expanding at a rate $\sim2\alpha k_0$ lattice vectors per unit time; when in-phase islands meet, they coalesce; when out-of-phase islands meet, a domain boundary is formed; in either case, growth continues at the same rate perpendicular to the free perimeter. For perfectly circular islands, the domain boundaries formed would be sections of hyperbolae.[16] Here they are per-

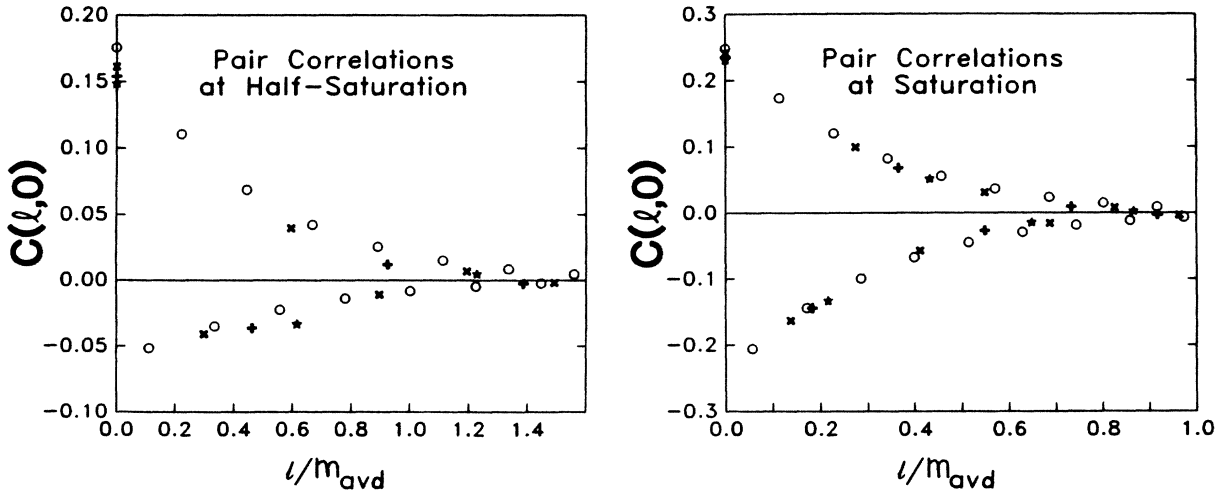

FIG. 10. $C(l,0)$ vs $l/m_{\mathrm{av}\,d}$ for $c(2\times2)$ islands at half-saturation and saturation. Results are shown for $k_i \propto \alpha^i$ with $\alpha=1$ (★), 2 (+), 5 (×), and 40 (○).

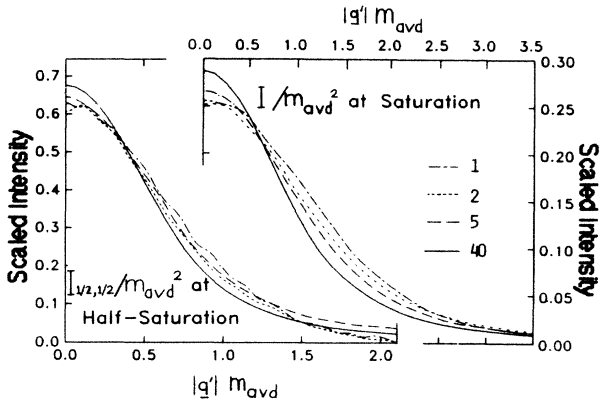

FIG. 11. $I_{1/2,1/2}/m_{av\,d}^2$ vs $m_{av\,d}\,|\,\mathbf{q}'\,|$ at half-saturation and saturation for $c(2\times2)$ islands formed by chemisorption with rates $k_i \propto \alpha^i$, and various α (shown).

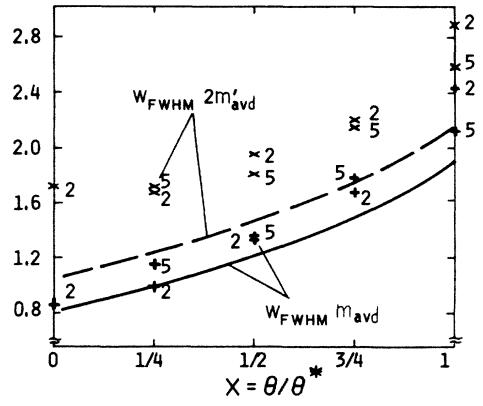

FIG. 12. $W_{\mathrm{FWHM}}m_{av\,d}$ and $W_{\mathrm{FWHM}}2m'_{av\,d}$ vs $x=\Theta/\Theta^*$ for $c(2\times2)$ island formation with rates $k_i \propto \alpha^i$. Curves correspond to large-α ($=40$) behavior, and some $\alpha=2$ and 5 values are shown. The FWHM is measured along $\mathbf{q}'=(q',q')$, and values for $\alpha=2$ were taken where I was midway between its maximum and minimum values (more sophisticated deconvolution was ambiguous here).

turbed from this form by lattice effects, noncircularity of islands, and fluctuations at island perimeters on a (small) length scale $O(w)$ [see Fig. 13, and Fig. 18(b) below].

Using this picture[7] one can show that the characteristic or scaling length, ξ, and characteristic time, τ, satisfy $\xi \sim c(\Theta)\alpha^{1/3}$, where $c \sim \Theta^{1/3}$ as $\Theta \to 0$, and $\tau \sim k_0^{-1}\alpha^{-2/3}$. Complete information on the large-α self-similar structure, including scaling functions, is determined by a continuum two-state Johnson-Mehl–type model:[7,16] grains nucleate at constant rate at empty points in the plane, and are randomly assigned one of two phases; they have nearly circular shape and expand at a constant rate; when grains meet, they merge if of like phase, and form a domain boundary otherwise, and growth at free boundaries continues at the same rate. We caution that this limiting structure is only achieved for very large α (cf. Fig. 13), but we shall see that large-α scaling forms for the correlations and diffracted intensity are achieved relatively quickly.

We have previously shown that m'_{av} scales like α^{ν}, where $\nu=\frac{1}{3}$ at saturation, and $\nu\approx\frac{1}{5}$ below saturation (at least for $\alpha \lesssim 200$) at fixed Θ. Also, $\alpha^{-1/3}$ scaling of $\frac{1}{2}-\Theta^*$ was demonstrated.[7] To understand these results, consider first the low-Θ regime of separated islands with $R=O(\xi)\sim O(\alpha^{-1/3})$. We expect that the defects (i.e., holes, overhangs) encountered in any one-dimensional cross section of the island are mainly in the growing zone, but increase in number with increasing R perhaps like $O(w)$. These have the effect of reducing m'_{av} (or $m'_{av\,d}$) from $O(R)$ to something like $O(R/w)=O(R^{1-p}) \sim \alpha^{(1-p)/3}$. (These arguments are crude since we do not distinguish between "intrinsic" width, and that due to long-wavelength fluctuations.[23] The former relates more to defects, and use of an associated effective p, for the "small" clusters analyzed here, may be appropriate.)

TABLE I. Island-size measure and peak superlattice beam intensity behavior for $c(2\times2)$ island formation with multiplicative rates $k_i \propto \alpha^i$. See Table III for $\alpha=1$.

α	Θ/Θ^*	m_{av} (m'_{av})	$m_{av\,d}$ ($m'_{av\,d}$)	$I(\pi,\pi)$
40	$\frac{1}{4}$	3.77 (2.37)	5.65 (3.56)	30
	$\frac{1}{2}$	6.00 (3.50)	8.98 (5.45)	55
	$\frac{3}{4}$	8.29 (4.69)	12.5 (7.43)	75
	1	10.8 (6.09)	17.5 (9.8)	88
5	$\frac{1}{4}$	1.51 (1.26)	2.08 (1.55)	3.7
	$\frac{1}{2}$	2.30 (1.66)	3.35 (2.22)	7.3
	$\frac{3}{4}$	3.32 (2.18)	4.94 (3.06)	10.5
	1	4.62 (2.86)	7.27 (4.25)	14.1
2	$\frac{1}{4}$	1.25 (1.13)	1.46 (1.23)	1.89
	$\frac{1}{2}$	1.68 (1.34)	2.16 (1.58)	3.20
	$\frac{3}{4}$	2.38 (1.69)	3.30 (2.16)	5.23
	1	3.53 (2.27)	5.46 (3.23)	7.51

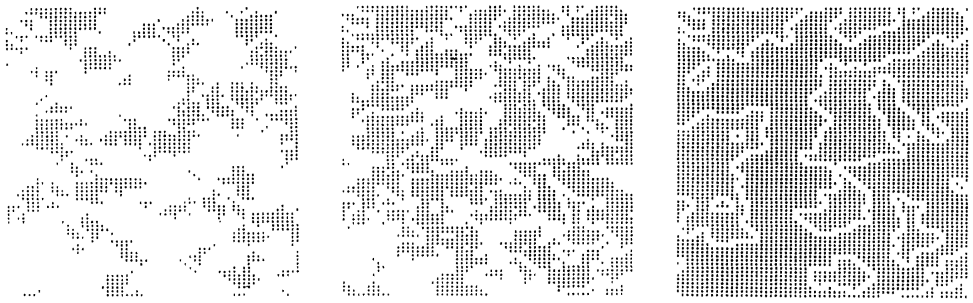

FIG. 13. Computer simulations of $c(2\times2)$ island formation for chemisorption with Eden rates $k_i=200k_0$, $i\geq1$, for $x=\Theta/\Theta^*=\frac{1}{3},\frac{2}{3},1$. X, Y, and ○ as in Fig. 9.

Such scaling is also expected for higher Θ where island coalescence is significant, but broad growing zones still are present. However, at saturation the defects in the growing zone have been "filled in" so m'_{av} (or m'_{avd}) again scales like $\xi\sim\alpha^{1/3}$. Thus m'_{av} (or m'_{avd}) is a suitable candidate for the scaling length, ξ, at saturation, but *not* below. Although defects should not cause m_{av} (or m_{avd}) to scale differently from ξ for large α (these averages have an additional length weighting), their effect will still be significant for the α range considered here.

These remarks suggest that a more appropriate measure of island size, i.e., number of atoms, associated with one-dimensional cross sections would ignore any defects associated with individual growing $c(2\times2)$ islands. These new size measures which we denote by $\tilde{m}_{av},\tilde{m}'_{av},\ldots$, corresponding to $m_{av},m'_{av},\ldots$, are clearly larger than the latter below saturation and, in fact, scale like $\xi\sim C\alpha^{1/3}$. Of course, at saturation where there are no defects within $c(2\times2)$ domains, one has $\tilde{m}_{av}=m_{av}$, etc. We also set $\tilde{m}_{av}=m_{av}$, etc., for $\alpha=1$ where we interpret all defects to be between domains. Figure 14 contrasts the coverage dependence of these various size measures for $\alpha=200$.[24] These new size measures can be used for the scaling length below (and at) saturation.

We now analyze spatial-correlation and diffracted intensity behavior for $\alpha=1,3,9,200$ to assess how quickly the high-α scaling form is achieved. Note that $\alpha=1$ Eden and multiplicative rate choices coincide. Figure 15 shows $C(l,0)$ versus l/m_{av} at saturation. The high-α form is achieved for $\alpha\gtrsim50$. $C(l,l)\geq0$ scales similarly. Figure 16 shows $(I=I_{1/2,1/2})/m^2_{avd}$ versus $m_{avd}|\mathbf{q}'|$, for $\mathbf{q}'=(q',q')$, at saturation. Behavior for $\mathbf{q}'=(q',0)$ is similar, except for larger $\alpha=1$ undulations. Replacing m_{avd} by m_{av} (m'_{avd} or m'_{av}) produces equally (almost as) good low-α scaling. We have checked that corresponding correlation and diffracted intensity scaling (using m_{av}, m_{avd}, etc.) breaks down *below saturation,* as explained above. On the other hand, using $\tilde{m}_{avd}$ as the scaling length seems to produce a dramatic improvement. For example, at half-saturation, the ratio of $I(\pi,\pi)$ for $\alpha=200$ to $\alpha=1$ equals ~19, whereas the corresponding ratio of $\tilde{m}^2_{avd}$ (m^2_{avd}) equals ~21 (~11). Also, the product of the FWHM of $I_{1/2,1/2}$ for diagonal cross sections with $\tilde{m}_{avd}$ (m_{avd}) equals 1.2π (0.86π), for $\alpha=200$, and both equal 1.5π, for $\alpha=1$. Scaling at half-saturation for

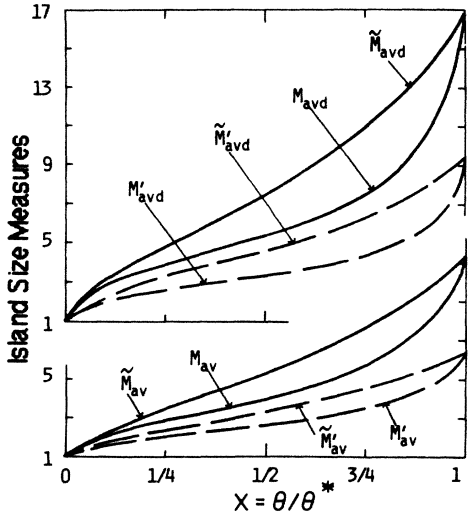

FIG. 14. Coverage ($\Theta=x\Theta^*$) dependence of various quasi-one-dimensional island-size measures for $c(2\times2)$ island formation with Eden rates, $k_i=200k_0$, $i\geq1$.

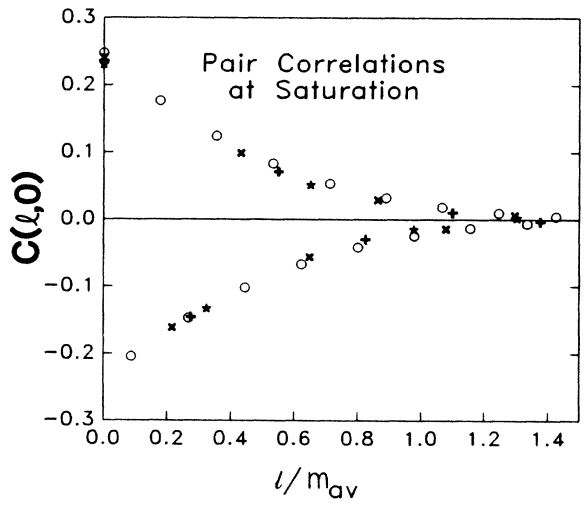

FIG. 15. $C(l,0)$ vs l/m_{av} for $c(2\times2)$ islands at saturation. Results are shown for $k_i=\alpha k_0$, $i\geq1$, with $\alpha=1$ (★), 3 (+), 9 (×), and 200 (○).

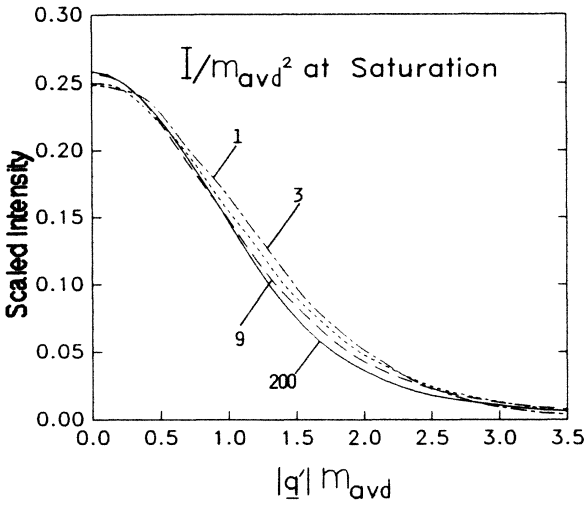

FIG. 16. $I_{1/2,1/2}/m_{av\,d}^2$ vs $m_{av\,d}|\mathbf{q}'|$ at saturation for $c(2\times2)$ islands formed by chemisorption with rates $k_i=\alpha k_0$, $i\geq1$, and various α (shown).

$\alpha=200$ using $\tilde{m}_{av}$, $\tilde{m}'_{av\,d}$, or $\tilde{m}'_{av}$ is much poorer, but still improved over using m_{av}, $m'_{av\,d}$, or m'_{av}, respectively. Finally, we note that choosing the scaling length as $I(\pi,\pi)^{1/2}$ produces excellent low-α scaling for fixed Θ/Θ^*, and at saturation (as well as excellent scaling with varying Θ, for fixed α). The coverage dependence of the FWHM of $I_{1/2,1/2}$, as well as the peak intensity, and the corresponding $\tilde{m}$ quantities, are given in Table II for $\alpha=200$. Behavior is similar to that seen in subsection A (Fig. 12 and Table I). A discussion of effects of coalescence follows in subsection C.

C. Effect of coalescence on island-size measures

Clearly, at low Θ, the increase in island size is predominantly due to growth of separated islands, whereas near saturation the contribution from coalescence is significant (the chance two islands coalesce upon meeting is $\sim\frac{1}{2}$). The quantitative effect of coalescence depends greatly on the size measure, and is best analyzed by comparing "parallel" processes with and without coalescence, denoted (C) and (NC), respectively. We focus on the *strongly clustering regime,* where $I(\mathrm{C})\sim I(\mathrm{NC})$.

Here the ratios $\tilde{m}'_{av}(\mathrm{C})/\tilde{m}'_{av}(\mathrm{NC})$ and $\tilde{m}'_{av\,d}(\mathrm{C})/\tilde{m}'_{av\,d}(\mathrm{NC})$ approach 1, as $\Theta\to0$, and equal 2 at saturation. Corresponding unprimed ratios vary from 1, at low Θ, to nontrivial limits (probably somewhat above 2) at saturation. The $\tilde{m}$ quantities can be replaced by m quantities for islands with narrow growing zones. Thus, from the above discussion, we see that the decrease in the FWHM (or increase in peak intensity) of the superlattice beam with Θ seems to reflect quite accurately the increase in the $\tilde{m}$ quantities, particularly $\tilde{m}_{av\,d}$ (to within a "coalescence factor" of ~2) (cf. Sec. II).

Clearly the effect of coalescence on s_{av}, or average radii of gyration, will be much more dramatic near saturation. Consequently, s_{av} will increase much more quickly than $I(\pi,\pi)$ near saturation, and the superlattice beam FWHM will decrease much more slowly than the reciprocal of the average radius of gyration. We now give a more concise analysis of these effects for the Eden rate choice, focusing on the structure of the *saturation state.* First, note that $c(2\times2)$ percolation is not possible here for reasons of topology and symmetry.[8,18] However, as the clustering propensity, i.e., α, gets larger, the saturation state becomes "closer to percolating" (see Ref. 8 for a concise definition), and its domain fractal dimension approaches the random percolation value of 1.89. Thus as α increases, the average domain radius of gyration, and size, increase *relative to* the correlation length, ξ, and ξ^2, respectively. The $\alpha\to\infty$ strongly clustering limit is described by a two-state Johnson-Mehl–type grain growth model, as mentioned above. See Ref. 7 and Fig. 18(b) for a picture of the saturation state. Arguments from random lattice and continuum percolation theory, as well as some lattice-model calculations,[8] suggest that the saturation state may even be at the percolation threshold here, i.e., s_{av} and the average radius of gyration have actually diverged.

D. Random filling with NN blocking ($\alpha=1$): A model for metastable $c(2\times2)$O/Fe(001)

Exposure of Fe(001) to water vapor at temperatures from 298 to 473 K produces a disordered $c(2\times2)$ oxygen overlayer. It was proposed that evolution of this oxygen adlayer, and its saturation state, could be described by random filling with NN blocking.[14] We have discussed the kinetics of this model previously.[18] Table III contrasts the coverage dependence of $I(\pi,\pi)$, the FWHM of the superlattice beam along $\mathbf{q}'=(q',q')$ (d) and $\mathbf{q}'=(q',0)$ (h), and measures of domain size, m_{av}, etc. The correlation is reasonable. On the other hand, in this model, s_{av} (~1 for $\Theta\sim0$) increases to ~165,[8] and the average domain radius of gyration (~0 for $\Theta\sim0$) in-

TABLE II. Island-size measure and diffracted intensity behavior for $c(2\times2)$ island formation with $\alpha=200$ Eden rates. Superlattice beam FWHM values in $\mathbf{q}$ space (in units of π) are measured along $\mathbf{q}'=(q',q')$ (d) and $\mathbf{q}'=(q',0)$ (h).

Θ/Θ^*	$\tilde{m}_{av}$ $(\tilde{m}'_{av})$	$\tilde{m}_{av\,d}$ $(\tilde{m}'_{av\,d})$	$I(\pi,\pi)$	$W_{\mathrm{FWHM}}(d)$	$[W_{\mathrm{FWHM}}(h)]$
$\frac{1}{4}$	3.4 (2.4)	4.9 (3.2)	23	0.201	(0.200)
$\frac{1}{2}$	5.2 (3.3)	7.5 (4.6)	38	0.160	(0.155)
$\frac{3}{4}$	7.6 (4.6)	10.9 (6.4)	54	0.139	(0.135)
1	11.4 (6.4)	16.7 (9.4)	73	0.132	(0.127)

TABLE III. Island-size measure and diffracted intensity behavior for random filling with NN blocking modeling $c(2\times2)$O/Fe(001). Superlattice beam FWHM values in **q** space (in units of π) are measured where I is midway between its maximum and minimum values along the chosen directions.

Θ/Θ^*	m_{av} (m'_{av})	$m_{av\,d}$ $(m'_{av\,d})$	$I(\pi,\pi)$	$W_{FWHM}(d)$	$[W_{FWHM}(h)]$
0	1 (1)	1 (1)	1	1.41	(1.00)
$\frac{1}{4}$	1.22 (1.11)	1.23 (1.12)	1.38	1.15	(0.84)
$\frac{1}{2}$	1.53 (1.27)	1.63 (1.31)	2.01	0.92	(0.79)
$\frac{3}{4}$	2.04 (1.52)	2.44 (1.72)	3.20	0.71	(0.69)
1	3.07 (2.03)	4.62 (2.76)	5.46	0.57	(0.54)

creases to ~ 22, at saturation[25] (see Fig. 17). Clearly the dramatic increase in these quantities is not reflected in diffracted intensity behavior. Recall that effects of coalescence here (for $\alpha=1$) should be less than for $\alpha>1$, where saturation states are "closer to percolating."

Finally, we note that for the lattice-filling models considered here, and no doubt others, spatial pair-correlation behavior should exhibit a crossover from its scaling form, on length scales $O(\xi)$, to a faster superexponential asymptotic decay for larger separations.[14] The latter is most easily seen for random filling with NN blocking ($\alpha=1$) where ξ is smallest and where, at saturation, $\Theta^*=0.364$, and we find that $-(l+2)C(l+1,0)/C(l,0)$ equals 1.14, 1.17, 1.09, 0.96, . . . , for $l=0,1,2,3,\ldots$. This fast asymptotic decay does not influence the large-α scaling forms for pair correlations or diffracted intensity, and seems to have little influence for finite α.

IV. CONCLUSIONS AND EXTENSIONS

For nonequilibrium $c(2\times2)$ ordering during chemisorption, we have identified quasi-one-dimensional measures of island size which can be used as scaling lengths. We have analyzed the scaling of pair correlations and diffracted intensities associated with self-similarity for a class of models with varying island sizes, for fixed coverage or at saturation. For any one of these chemisorption processes, we have shown that the variation with coverage of the superlattice beam FWHM and peak intensity reflect only the component of the increase in $c(2\times2)$ domain size *not* associated with coalescence. Thus they do not reflect the dramatic increase in domain size near saturation where island coalescence is significant, or the associated percolative domain structure. Near saturation we observe a dramatic diminution in the integral-order beam intensity (for scattering from the adlayer only). The associated cancellation in the sum over correlations is also reflected in the scaling theory.[26]

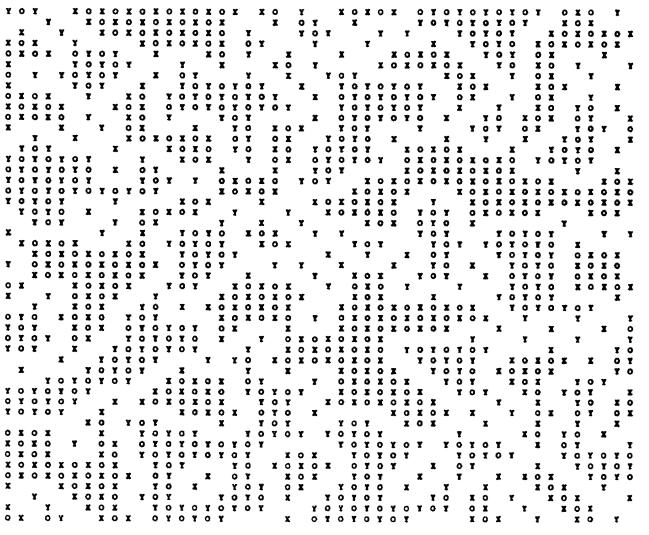

FIG. 17. Computer simulation of the saturation state for random filling with NN blocking ($\alpha=1$) modeling $c(2\times2)$O/Fe(001). X, Y, and ○ as in Fig. 9.

Although we have analyzed only one type of model for $c(2\times2)$ ordering during chemisorption, we expect that our conclusions are general, since there will always be significant coalescence near saturation. Here we briefly remark on some other possible models. Suppose $c(2\times2)$ clusters are nucleated only at randomly distributed "defects" of density ε, and then grow with Eden rates. Then for $\varepsilon\ll1$ the process is described by a two-phase cell-type model:[16] at $t=0$, nearly circular grains start to grow at constant rate about seeds randomly distributed in the plane; they are randomly assigned one of two phases; when grains meet, they merge if of like phase, and form a domain boundary otherwise. The corresponding saturation state is represented in Fig. 18(a). In a quite different model, one might assume that $c(2\times2)$ islands are nucleated at constant rate from density fluctuations in a "gas" of chemisorbed particles, and thereafter grow a constant rate. However, one might anticipate depletion of the "gas" density near growing clusters, which would inhibit nucleation in that region.[27] Thus the continuum picture is the same as in Sec. III C, except that now nucleation is forbidden in a depletion zone surrounding growing grains. See Fig. 18(c) for the saturation state. Other models with modified growth rates[27] would also produce percolative saturation states. The similarity of large-scale structure of all these saturation states reflects a presumably universal percolation class.[8]

We also mention the "eight-site model" involving the random filling of NNN pairs of empty sites for which all six NN's are empty.[28] Such a model, with either limited or no subsequent adatom mobility, has been proposed to describe the formation of metastable $c(2\times2)$O/Pd(100) under conditions of low temperature and high pressure.[18,29] For the immobile model, in the saturation

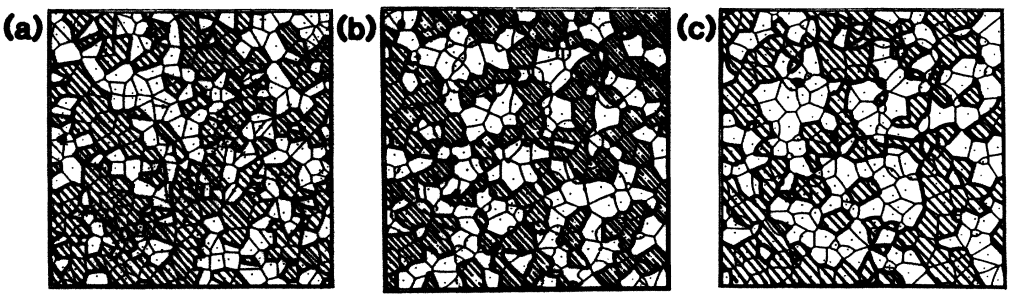

FIG. 18. Saturation states for two-phase versions of (a) the cell model (growth of circular grains about defects), (b) the Johnson-Mehl model (continuous nucleation of circular grains), and (c) the Johnson-Mehl model with a nucleation-free zone around each growing grain of width $0.2A^{1/2}$, where A is the final grain area. Grain expansion always occurs at constant rate. These grain patterns, from Ref. 27, show all nuclei as points, and boundaries as light lines. Each grain is randomly assigned one of two phases, and domains of one phase are shown cross-hatched.

state, one finds that[18,25,30] $m_{\rm av}=3.5$, $m'_{\rm av}=2.3$, $m_{{\rm av}\,d}=4.8$, $m'_{{\rm av}\,d}=3.0$, $s_{\rm av}\sim280$, $R_{\rm av}(2)=28$, $R_{\rm av}(1)=18$, $I(\pi,\pi)=9.7$, $W_{\rm FWHM}(d)=0.36\pi$, and $W_{\rm FWHM}(h)=0.35\pi$. Behavior here is very similar to that seen including limited mobility, or for random filling of single sites with NN blocking (Sec. III D). For example, due to coalescence, $s_{\rm av}$ is always much larger than $I(\pi,\pi)$ at saturation.

Finally, we comment on nonequilibrium ordering processes analogous to those considered here, but where islands have more than two phases [e.g., fourfold degenerate $p(2\times1)$ ordering]. Scaling relations for the spatial correlations and diffracted intensity could be developed analogous to those discussed here for $c(2\times2)$ islands. However, the effect of coalescence on domain sizes would be substantially less dramatic. On the other hand, for analogous processes in three dimensions with two-phase domains (e.g., the two-state Johnson-Mehl model), a percolation transition will no doubt occur before saturation. Here the domain size diverges, but the diffracted intensity behaves smoothly.

ACKNOWLEDGMENTS

Ames Laboratory is operated for the U.S. Department of Energy by Iowa State University under Contract No. W-7405-ENG-82. This work was supported by the Division of Engineering, Mathematics, and Geosciences, with Budget Code No. KC-04-01-03. One of us (J.A.R.) was supported by the 1987 Ames Laboratory undergraduate student trainee program.

APPENDIX A: SECOND-ORDER SPATIALLY MARKOVIAN DISTRIBUTIONS IN 1D

Here the state of a site $\sigma=$o or x is influenced by the state of the pair $\sigma_1\sigma_2$ to the right (or left), but not more distant sites. Thus 2^2 conditional probabilities $P[{\rm x}|\sigma_1\sigma_2]$ (or $P[{\rm o}|\sigma_1\sigma_2]$) of finding x (o) given the adjacent pair, $\sigma_1\sigma_2$, specify the model. Note that $P[{\rm o}|\sigma_1\sigma_2]+P[{\rm x}|\sigma_1\sigma_2]=1$. Define the $2^2\times2^2$ matrix $(\underline{T})_{\sigma_1\sigma_2,\sigma_3\sigma_4}=P[\sigma_1\,|\,\sigma_2\sigma_3]P[\sigma_2\,|\,\sigma_3\sigma_4]$, which trivially has an eigenvalue $\lambda=1$ corresponding to an equal-component dual eigenvector. Then the pair probability

$$P(l)=\sum_{\sigma_i}P[{\rm x}\,|\,\sigma_1\sigma_2]P[\sigma_1\,|\,\sigma_2\sigma_3]\cdots P[\sigma_{l-2}\,|\,\sigma_{l-1}{\rm x}]\ ,$$

and various other quantities, can be conveniently written in terms of powers of $\underline{T}$. We adopt previously used terminology for this "extended geometric" model,[31] and write $\gamma_{\rm x}=P[{\rm o}|{\rm xx}]$, $\gamma_{\rm o}=P[{\rm x}|{\rm oo}]$, $\sigma_{\rm x}=P[{\rm o}|{\rm xo}]$, and $\sigma_{\rm o}=P[{\rm x}|{\rm ox}]$.

We restrict our attention to the special case of *no* neighboring pairs of filled sites (xx), so $\gamma_{\rm x}=1$, $\sigma_{\rm x}=1$, $\gamma_{\rm o}=\Theta(1-2\Theta)^{-1}/s'_{\rm av}$ ($\equiv\gamma$, say), and $\sigma_{\rm o}=1-1/s'_{\rm av}$ ($\equiv\sigma$, say). $\underline{T}$ trivially has eigenvalues $\lambda=0$ and 1, and the two nontrivial eigenvalues, $\lambda^{\pm}$, satisfy

$$2\lambda^{\pm}=2\sigma-2\gamma+\gamma^2\pm\gamma(4\sigma-4\gamma+\gamma^2)^{1/2}\ .$$

One can show that, for $l\geq0$, here

$$\Theta^{-1}P(2l+1)=(\underline{T}^l)_{{\rm xo,ox}}\ ,$$

$$\Theta^{-1}P(2l+2)=\sigma(\underline{T}^l)_{{\rm ox,ox}}+\gamma(\underline{T}^l)_{{\rm oo,ox}}\ .$$

Thus, $I(q)=\Theta^{-1}\sum_l e^{iql}P(l)$, for $q\neq0(\mathrm{mod}\,2\pi)$, satisfies

$$I(q)-1=e^{iq}\underline{S}(q)_{{\rm xo,ox}}+\sigma e^{2iq}\underline{S}(q)_{{\rm ox,ox}}+\gamma e^{2iq}\underline{S}(q)_{{\rm oo,ox}}+{\rm c.c.}\ ,$$

where c.c. denotes complex conjugate, and $\underline{S}=(\underline{1}-e^{2iq}\underline{T})^{-1}$.

Now consider specifically the *large-island-size regime*, $s'_{\rm av}\gg1$. First, consider distributions for *fixed* $\theta<\frac{1}{2}$. Here we find that

$$\lambda^+\sim1-1/s'_{\rm av},\quad \lambda^-\sim1-[(1-2\Theta)s'_{\rm av}]^{-1}\ ,$$

$$C(l)\sim+(-)\frac{\Theta}{2}e^{-l/(2s'_{\rm av})}+\frac{\Theta}{2}(1-2\Theta)e^{-(1-2\Theta)^{-1}l/(2s'_{\rm av})}$$

for even (odd) l ,

$$I_0\sim\frac{2(1-2\Theta)^2s'_{\rm av}}{1+[2(1-2\Theta)qs_{\rm av}]^2}\quad\text{and}\quad I_{1/2}\sim\frac{2s'_{\rm av}}{1+(2q's'_{\rm av})^2}\ .$$

Second, consider distributions *at saturation* where no triples of empty sites exist, so $s'_{\rm av}=\Theta(1-2\Theta)^{-1}$ and $\gamma=1$. Here we find that

$$\lambda^{+}\sim 1-2/s'_{\rm av},\quad \lambda^{-}\sim (s'_{\rm av})^{-2},$$

$$C(l)\sim +(-)\tfrac{1}{4}e^{-l/s'_{\rm av}} \text{ for even (odd) } l,$$

$$I_0\sim 0 \text{ and } I_{1/2}\sim \frac{s'_{\rm av}}{1+(q's'_{\rm av})^2}.$$

One could extend these calculations to nth-order Markovian distributions, where $\underline{T}$ becomes a $2^n\times 2^n$ matrix. Eigenvalues satisfy $|\lambda|\le 1$, and include $\lambda=1$.[14] If there are *no* neighboring filled pairs, then $\underline{T}$ has an m-fold degenerate eigenvalue $\lambda=0$, where m is the number of distinct configurations of n consecutive sites which include a filled pair. In the large-island-size limit, $\lambda=1$ becomes degenerate. Degenerate Raleigh-Schrödinger perturbation theory can be readily extended to analyze the near-unity eigenvalues of the non-self-adjacent $\underline{T}$.[32]

APPENDIX B: TAYLOR EXPANSIONS IN Θ FOR $C(l)$ AND $I(\mathbf{q})$

Taylor expansions in Θ for the pair correlations immediately yield a corresponding expansion for the diffracted intensity. For the nonequilibrium irreversible cooperative filling models considered here, such expansions can be determined directly,[33,34] and a diagrammatic characterization of the coefficients is even available for the multiplicative rate choice $k_i\propto\alpha^i$.[33] In general, it is most efficient to determine these via auxiliary t expansions for the Θ and $C(l)$, finally eliminating t.[18] The last procedure applies to general lattice adsorption models (including desorption and hopping). Clearly, the order of the lead term will increase with separation, l.[34]

For the linear lattice model of Sec. II, we find that $C(0)=\Theta-\Theta^2$, $C(1)=-\Theta^2$, $C(2)=(\alpha-1)\Theta^2+2\alpha(3-2\alpha)\Theta^3/3+\cdots$, $C(3)=-8(\alpha-1)\Theta^3/3+\cdots$, and $C(4)=4(\alpha-1)^2\Theta^3/3+\cdots$. $C(2l)$ and $C(2l-1)$ are $O(\Theta^l)$, for $l\ge 2$, so these results determine $\Theta I(q)=C(0)+2\sum_{l=1}^{\infty}C(l)\cos(lq)$ to within $O(\Theta^4)$. For the square-lattice model of Sec. III, we find that $C(0,0)=\Theta-\Theta^2$, $C(1,0)=-\Theta^2$; $C(1,1)-(\alpha-1)\Theta^2=\alpha(16-9\alpha)\Theta^3/3\cdots$ for multiplicative (M) rates and $4\alpha(2-\alpha)\Theta^3/3+\cdots$ for Eden (E) rates; also, $C(2,0)=2(\alpha^2-4\alpha+3)\Theta^3/3+\cdots$, $C(2,1)=-4(\alpha-1)\Theta^3/3+\cdots$, and $C(2,2)=2(\alpha-1)^2\Theta^3/3+\cdots$ for both M and E rates, but differences appear in higher-order terms. Other $C(l)$ are $O(\Theta^n)$, with $n\ge 4$,[34] so these results determine

$$\Theta I(\mathbf{q})=C(0,0)+2C(1,0)(\cos q_x+\cos q_y)+4C(1,1)\cos q_x\cos q_y$$
$$+4C(2,1)[\cos q_x\cos(2q_y)+\cos(2q_x)\cos q_y]+4C(2,2)\cos(2q_x)\cos(2q_y)+\cdots$$

to within $O(\Theta^4)$.

Finally, note that if we replace α by $e^{-\varepsilon/(k_BT)}$, then the $C(l)$ expansions for *multiplicative* rates correspond to $C(l)$ virial expansions for an equilibrated lattice gas (on a square lattice, with NN infinite repulsions and NNN interactions ε, at temperature T) up to $O(\Theta^3)$, but there are discrepancies in $O(\Theta^4)$ terms.[33]

*Present address: Department of Chemistry, Eastern Michigan University, Ypsilanti, Michigan 48197. Formerly at Department of Chemistry, Iowa State University, Ames, IA 50011.

[1]G. A. Somorjai, *Chemistry in Two Dimensions: Surfaces* (Cornell University Press, Ithaca, 1981).

[2]M. G. Lagally, G.-C. Wang, and T.-M. Lu, CRC Crit. Rev. Solid State Mater. Sci. **7**, 233 (1978).

[3]W. H. Weinberg, Annu. Rev. Phys. Chem. **34**, 217 (1983); D. P. Woodruff, G.-C. Wang, and T.-M. Lu, in *Chemistry and Physics of Solid Surfaces,* edited by D. A. King and D. P. Woodruff (Elsevier, Amsterdam, 1983), Vol. 2; L. D. Roelofs, in *Chemistry and Physics of Solid Surfaces,* edited by R. Vanselow and R. Howe (Springer, Berlin, 1982), Vol. 4; T. L. Einstein, *ibid.*

[4]See, for example, J. D. Gunton and K. Kaski, Surf. Sci. **144**, 290 (1984); M. Tringides, P. K. Wu, and M. G. Lagally, Phys. Rev. Lett. **59**, 315 (1987).

[5]E. D. Williams, W. H. Weinberg, and A. C. Sobrero, J. Chem. Phys. **76**, 1150 (1982); E. D. Williams and W. H. Weinberg, Surf. Sci. **109**, 574 (1981).

[6]E. S. Hood, B. H. Toby, and W. H. Weinberg, Phys. Rev. Lett. **55**, 2437 (1985).

[7]J. W. Evans and R. S. Nord, J. Vac. Sci. Technol. A **5**, 1040 (1987); J. W. Evans, J. A. Bartz, and D. E. Sanders, Phys. Rev. A **34**, 1434 (1986).

[8]J. W. Evans and D. E. Sanders, J. Vac. Sci. Technol. A **6**, May/June (1988) and unpublished.

[9]W. W. Mullins and R. F. Sekerka, J. Appl. Phys. **34**, 323 (1963).

[10]M. A. Van Hove, W. H. Weinberg, and C.-M. Chan, *Low-Energy Electron Diffraction* (Springer-Verlag, Berlin, 1986).

[11]G.-C. Wang and T.-M. Lu, Phys. Rev. B **28**, 6795 (1983).

[12]J. W. Evans and R. S. Nord, Phys. Rev. B **35**, 6004 (1987).

[13]J. W. Evans and D. R. Burgess, J. Chem. Phys. **79**, 5022 (1983); R. S. Nord, D. K. Hoffman, and J. W. Evans, Phys. Rev. A **31**, 3820 (1985).

[14]J. W. Evans, D. R. Burgess, and D. K. Hoffman, J. Math. Phys. **25**, 2527 (1984).

[15]D. J. Dwyer, G. W. Simmons, and R. P. Wei, Surf. Sci. **64**, 617 (1977).

[16]W. A. Johnson and R. F. Mehl, Trans. AIME **135**, 416 (1939); S. Ohta, K. Ohta, and K. Kawasaki, Physica A **140**, 478 (1987).

[17]For $\alpha=1$ at half-saturation, I is concave at $q=0$, so we just set

$I_0 = I(q=0)$. Resulting $I_{1/2}$ scaling is poor.

[18]J. W. Evans, J. Chem. Phys. **87**, 3038 (1987).

[19]*On Growth and Form,* edited by H. E. Stanely and N. Ostrowsky (Nijhoff, Dordrecht, 1986).

[20]See J. W. Evans and H. Pak, Surf. Sci. (to be published) for a detailed discussion of time scales.

[21]For $\alpha=1$, we just set $I_{0,0} \equiv I(\mathbf{0})$.

[22]The size, s, of a single diamond-shaped island equals m^2, where m is the number of filled sites along an edge. Thus, for a distribution of sizes $s_{\rm av} = \langle m^2 \rangle \geq \langle m \rangle^2 = m^2_{{\rm av}\,d}$.

[23]M. Plischke and Z. Racz, Phys. Rev. A **32**, 2825 (1985); P. Freche, D. Stauffer, and H. E. Stanley, J. Phys. A **18**, L1163 (1985); D. E. Wolf, *ibid.* **20**, 1251 (1987); D. E. Wolf and J. Kertesz, *ibid.* **20**, L257 (1987).

[24]Our determination of $\tilde{m}$ quantities here is imprecise. For $\alpha=200$, we take filled sites in

```
                o
  x o x and x o o o x
                o
```

to be in the same domain, as well as those in

```
          x
    x,    o
  x   x
```

(the middle site must fill at saturation), and

```
        x
      o
    o
  x
```

(with probability $1-\Theta/\Theta^*$ for the latter). Thus we assume that short gaps in the perfect $c(2\times2)$ structure are within islands.

[25]Let $R_{\{s\}}$ be the radius of gyration (measured in units of lattice vectors) for domain $\{s\}$. Define $R^2_{\rm av}(i) = \sum R^2_{\{s\}} s^i n_{\{s\}} / \sum s^i n_{\{s\}}$. Then, for random filling with NN blocking ($\alpha=1$) at saturation, one has $R_{\rm av}(2) \sim 22$, $R_{\rm av}(1) \sim 13$, and $s_{\rm av} \sim 165$.

[26]This cancellation also corresponds to reduced fluctuations in the number, N, of adatoms, at fixed t, as saturation is approached. For an $L\times L$ lattice, one has $\sum_l C(l) = L^{-2}\langle (N - \langle N \rangle)^2 \rangle$, where $\langle\ \rangle$ is the ensemble average [cf. H. E. Stanley, *Phase Transitions and Critical Phenomena* (Oxford University Press, Oxford, 1971), p. 98].

[27]H. J. Frost and C. V. Thompson, Acta Metall. **35**, 529 (1987); H. J. Frost and C. V. Thompson, presented at 31st SPIE Symposium, San Diego, 1987 (unpublished).

[28]C. R. Brundle, R. Behm, and J. A. Barker, J. Vac. Sci. Technol. A **2**, 1038 (1984).

[29]S.-L. Chang and P. A. Thiel, Phys. Rev. Lett. **59**, 296 (1987).

[30]S.-L. Chang, D. E. Sanders, J. W. Evans, and P. A. Thiel, in *The Structure of Surfaces II,* Vol. 11 of *Springer Series in Surface Science,* edited by J. F. Van der Veen and M. A. Van Hove (Springer, Berlin, 1988).

[31]J. M. Pimbley, T.-M. Lu, and G.-C. Wang, J. Vac. Sci. Technol. A **4**, 1357 (1986).

[32]M. Reed and B. Simon, *Methods of Modern Mathematical Physics IV* (Academic, New York, 1978).

[33]D. K. Hoffman, J. Chem. Phys. **65**, 95 (1976).

[34]J. W. Evans, Physica **123A**, 297 (1984).